Available online at www.sciencedirect.com
ScienceDirect
Surface & Coatings Technology 202 (2008) 4114–4120
SURFACE & COATINGS TECHNOLOGY
www.elsevier.com/locate/surfcoat

Aligned multi-walled carbon nanotubes on different substrates by floating catalyst chemical vapor deposition: Critical effects of buffer layer

Hao Liu [a], Yong Zhang [a], David Arato [a], Ruying Li [a], Philippe Mérel [b], Xueliang Sun [a,*]

[a] Department of Mechanical and Materials Engineering, University of Western Ontario, London, ON, Canada N6A 5B9
[b] Defence Research & Development Canada – Valcartier, 2459 Boulevard Pie-XI nord, Québec, QC, Canada G3J 1X5

Received 13 December 2007; accepted in revised form 26 February 2008
Available online 8 March 2008

Abstract

Aligned multi-walled carbon nanotubes (MWCNTs) were synthesized by floating catalyst chemical vapor deposition on two types of substrates, with emphasis on the effects of an aluminum buffer layer. It has been revealed that the presence of the aluminum buffer layer on insulating/semiconducting silicon oxide/silicon wafer resulted in a higher growth rate, narrower diameter distribution, neater morphology and improved crystalline quality of MWCNTs. When an aluminum buffer layer is deposited on electrically conductive carbon paper, high yield CNTs can be achieved while no CNTs can be observed without this buffer layer. Morphology, structure and chemical states of the products were examined by field-emission scanning electron microscopy, transmission electron microscopy and X-ray photoelectron spectroscopy. The generation of alumina from the aluminum buffer layer is thought to play an important role in promoting the nanotube growth. Detailed growth mechanism of MWCNTs was also discussed.

Keywords: Chemical vapor deposition; Carbon nanotubes; Aluminum buffer; Field-emission scanning electron microscopy; Transmission electron microscopy; X-ray photoelectron spectroscopy

1. Introduction

Over the past 16 years since their discovery in 1991 [1], carbon nanotubes (CNTs) has attracted great interest due to their high strength [2,3], extraordinary flexibility [4,5], excellent electrical conductivity [6–8] and field emission properties [9,10], which promise tremendous applications in electron field emitter of displays [9,11], nanoscale electronic devices [12], biosensors [13], hydrogen storage [14] and fuel cell electrodes [15]. Among various approaches for growing CNTs, such as arc-discharge [1], laser ablation [16], and chemical vapor deposition method (CVD) [17,18], the CVD method has proven to be an effective method to generate large amount of CNTs as well as allowing direct growth of the nanotubes on pre-patterned substrates. Among the available CVD processes, floating catalyst (FC) CVD and aerosol-assisted (AA) CVD methods are exceptionally cheap and well-suited for scaling up to mass production of CNTs with a defined nanotube diameter distribution. Especially, FC-CVD has attracted considerable attention because it ensures continuous growth of aligned and high purity nanotubes, at a low reaction temperature, low cost and facile fabrication process [19]. Compared with traditional CVD method, the advantage of FC-CVD method is to allow the catalyst and carbon source to be introduced into the reactor simultaneously to produce well-aligned CNTs on various substrates, which is essential for nanodevice integration. Among different substrates, silicon (electrical semiconducting) and carbon microfibers (electrical conductive) are two representatives. The aligned growth of CNTs on silicon substrate provides the possibility of integrating CNTs directly into silicon technology while much high density CNTs on commercially-used carbon paper substrate can be used as Pt support electrodes for fuel cell applications [20–23].

However, there are significant challenges to synthesize high-quality CNTs on both substrates. Regarding CNTs on silicon substrate, a problem which arises is that undesired chemical interaction may occur between the catalyst and silicon substrate

* Corresponding author. Tel.: +1 519 661 2111x87759; fax: +1 519 661 3020.
E-mail address: xsun@eng.uwo.ca (X. Sun).

0257-8972/$ - see front matter © 2008 Elsevier B.V. All rights reserved.
doi:10.1016/j.surfcoat.2008.02.025

at high temperatures, which results in deterioration of the catalyst activity by the formation of a silicide [24]. To solve the problem, various intermediate buffer layers have been introduced [25,26] to increase the growth efficiency of the nanotubes and modify the catalyst-support interaction. However, the detailed role of buffer layers in CNTs growth still remains an unanswered question. As for CNTs on carbon paper, it is not easy to deposit catalytic nanoparticles on carbon fiber surface because of its hydrophobic nature. Therefore, other methods such as silane-assisted catalytic nanoparticle deposition method had to be used to obtain high-density CNTs on carbon paper [20,27,28].

In this paper, we used FC-CVD to synthesize clear, uniform and aligned MWCNTs with high crystallinity on silicon or carbon paper by introducing a thin aluminum film as the buffer layer. The chemical states of the catalyst and substrate at the initial nanotube growth stage have been investigated. The generation of a thin alumina layer during the heating process and the alumina-catalyst interaction are thought to promote the nanotube growth. Further, possible growth mechanism of the nanotubes was also discussed.

2. Experimental section

Before the growth of MWCNTs on silicon, a 300-nm-thick layer of SiO_2 on a p-type Si wafer was prepared by Plasma Enhanced Chemical Vapor Deposition (PECVD). Further, a thin aluminum buffer layer with a thickness of 10 nm was sputtered on top of the SiO_2 layer or bare carbon paper.

The floating catalyst CVD method was applied to synthesize MWCNTs based on a simple horizontal quartz tube furnace system by which temperature, carrier gas flow rate and growth time were controlled. Ferrocene ($Fe(C_5H_5)_2$, 98%, from Aldrich, 100 mg) used as the catalyst was placed at the entrance of the furnace in the quartz tube (ferrocene vaporization at 200 °C). A silicon (1.5 cm × 7 cm) wafer was put in the middle of the tube as a holder on which smaller and different substrates could be simultaneously located side-by-side. In our experiments, four different substrates were used: (1) Si wafer with a 300-nm-thick SiO_2 layer (marked as Si/SiO_2); (2) Si/SiO_2 with a 10-nm-thick aluminum layer (marked as $Si/SiO_2/Al$); (3) bare carbon paper; and (4) carbon paper with a 10 nm-thick aluminum layer.

Before the furnace was turned on, argon (99.999% in purity) was introduced into the heating system at a flow rate of 500 sccm for 30 min to eliminate the air in the tube. Then the system was heated at a rate of 60 °C/min. At the same time, ethylene gas was introduced into the system at a flow rate of 10 sccm with a constant Ar flow rate. Thus the ferrocene vapor was carried by the gas flow into the high temperature region where the pyrolysis of ferrocene and synthesis of the MWCNTs were performed at 850 °C. The whole system was kept at the

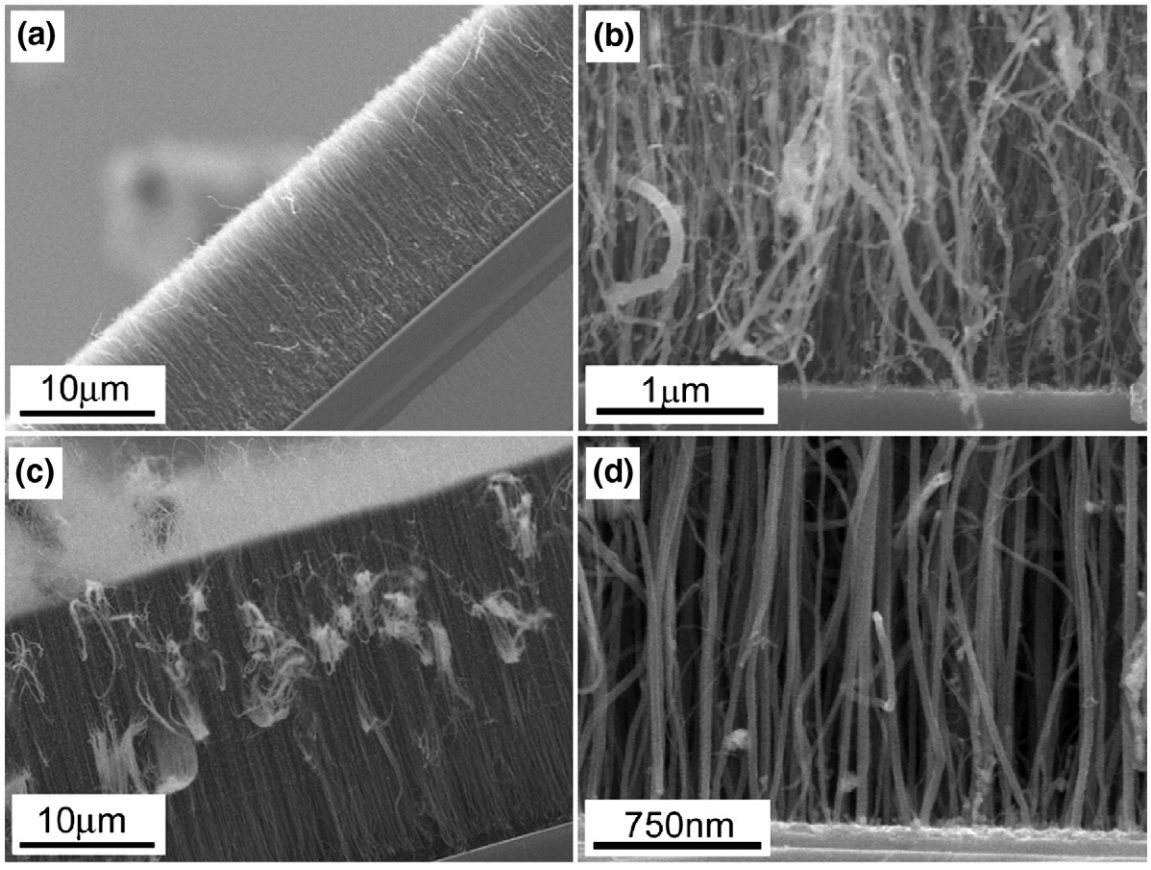

Fig. 1. SEM images of the MWCNTs grown on SiO_2 substrates without and with an aluminum buffer layer. a) and b) MWCNTs grown on a SiO_2 substrate without an aluminum buffer layer. c) and d) MWCNTs grown on a SiO_2 substrate with an aluminum buffer layer.

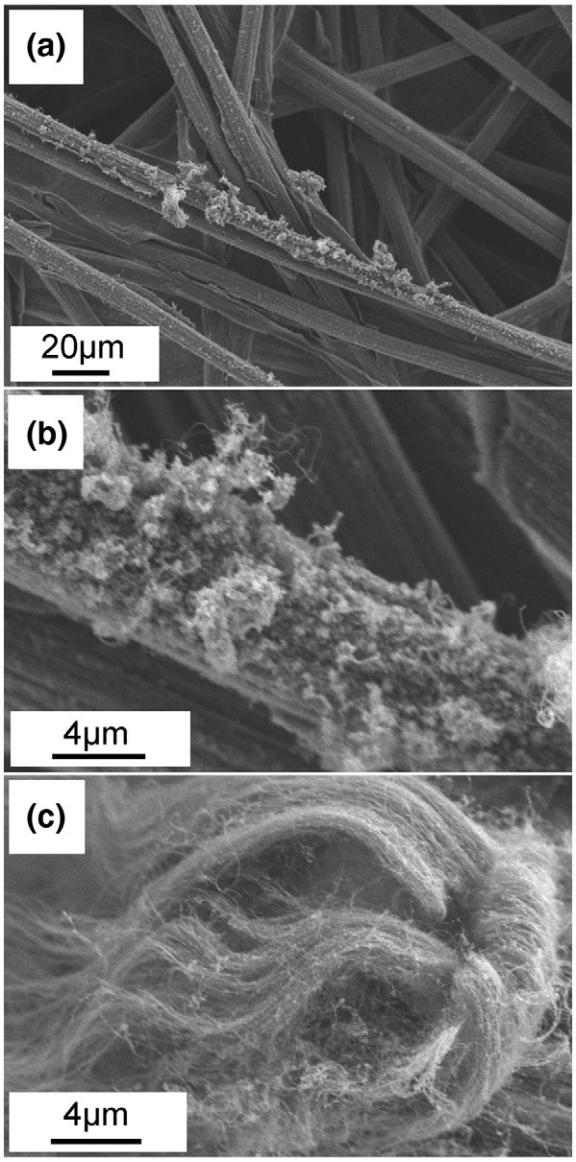

Fig. 2. SEM images of the a) and b) MWCNTs grown on a bare carbon paper. c) MWCNTs grown on a carbon paper with an aluminum buffer layer.

target temperature for 5 min, then the ethylene gas was turned off and the system cooled down to room temperature in the flowing Ar gas.

The samples were evaluated by Hitachi S-4500 field-emission scanning electron microscopy (FESEM) operated at 5.0 kV, JEOL 2010F transmission electron microscopy (TEM) operated at 200 kV, Kratos Axis Ultra Al(alpha) X-ray photoelectron spectroscopy (XPS) operated at 14 kV and Oxford INCA energy dispersive X-ray spectroscopy (EDX) operated at 10 keV.

3. Results and discussion

3.1. Morphological and structural analysis by SEM and TEM

Fig. 1 shows SEM images of the general morphology of MWCNTs. The aligned MWCNTs grown on the Si/SiO_2 substrate

Table 1
Summary of CNTs grown on different substrates with and without an aluminum buffer layer

Substrate	Si/SiO_2	$Si/SiO_2/Al$	Carbon paper	Carbon paper/Al
Growth rate (μm/min)	3	6	0	High-density but not alignment

are around 15 μm in length, as shown in Fig. 1(a). Further, the higher magnification SEM image in Fig. 1(b) clearly shows that there is a wide diameter distribution for the nanotubes grown on the Si/SiO_2 substrate and some particles are observed on the outer surface of the MWCNTs. While the Al buffer was employed, the length of the aligned nanotubes, around 30 μm, was achieved (Fig. 1(c)), suggesting a significantly higher growth rate compared with the case without the aluminum layer. Further, with the aluminum layer, the uniformity of the nanotube diameter is highly improved and outer surface of the nanotubes is clear and smooth (Fig. 1(d)).

Carbon paper is commercially used as fuel cell backing in proton exchange membrane fuel cells (PEMFCs) and direct methanol fuel cells (DMFCs) [29]. We found that the presence of the aluminum buffer layer is much more important for the growth of dense CNTs on carbon paper. Without aluminum buffer layer, shown as Fig. 2(a) and (b), few, short and curved CNTs are observed on some carbon fibers of carbon paper. However, when aluminum buffer layer is sputtered onto the surface of carbon paper, high density of CNTs are observed as shown in Fig. 2(c). In this case, carbon paper is totally covered by CNT bundles. Further, the bundle is composed of dense and oriented nanotubes (Fig. 2(c)). In this case, the length of the bundle is about 20 μm. However, we can not see whole length of the bundle and therefore we can not exactly calculate the growth rate of CNTs on carbon paper. This composite structure has great potential as Pt support in fuel cell electrodes, which is in progress in our group. Based on our SEM observation, the lengths of CNTs grown on different substrate are listed in Table 1. It displays that the growth rate of the nanotubes on the $Si/SiO_2/Al$ substrate is 6 μm/min, double that of the nanotubes on the Si/SiO_2 substrate.

TEM images in Fig. 3 show further structural details of MWCNTs grown on four kinds of substrates. It can be seen that, without the Al buffer layer, the nanotube diameter has a wider range (Fig. 3(a) and (c)), while the diameter distribution was a bit narrower in the presence of Al buffer layer (Fig. 3(b) and (d)). The diameters of these two kinds of CNTs are counted from 100 nanotubes under TEM images for each sample. Because it is difficult to harvest CNTs from the carbon paper substrate without Al buffer layer, we take the CNTs grown on the silicon substrate as the example to investigate the influence of buffer layer on the diameter distribution of the nanotubes. The diameter distributions of the CNTs grown on Si/SiO_2 and $Si/SiO_2/Al$ substrate are shown in Fig. 4. It is clear to see that without Al buffer layer the diameter of over 95% MWCNTs falls into a much wider size range from 5 to 85 nm. As a comparison, the diameter of over 95% nanotubes grown with an Al buffer layer is in the range of 25 – 65 nm. Furthermore, in the

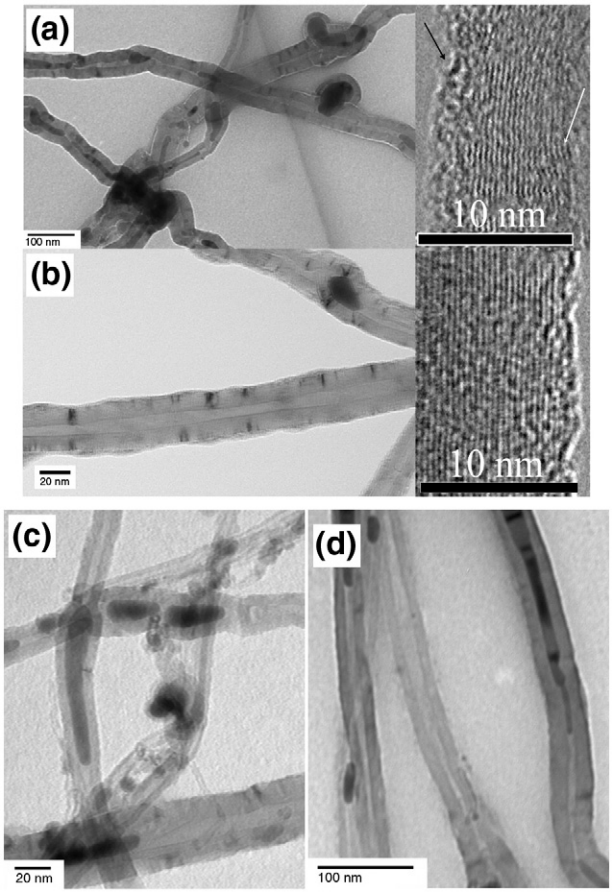

Fig. 3. TEM images of a) MWCNTs grown on a carbon paper without an aluminum buffer layer. Inset: HRTEM image showing the wall structure. b) MWCNTs grown on a carbon paper with an aluminum buffer layer. Inset: HRTEM image showing the wall structure. c) MWCNTs grown on Si/SiO_2 substrate and d) MWCNTs on Si/SiO_2/Al substrate.

absence of the Al buffer layer, many small particles with a diameter of ~50 nm can be observed on the outer surface of the nanotubes in Fig. 3(a). With the Al buffer layer, the nanotube's surface was very clean and straight. Some nanotubes were partly filled with catalyst particles for both cases shown in Fig. 3 (b) and (d). High resolution TEM images can give more detailed structural information of both nanotubes. The interplanar spacing of both nanotubes is determined to be 0.35 nm. However, the MWCNTs grown without using the Al buffer layer show more defects, such as distorted walls, discontinuation and amorphous component of the carbon nanotube walls (Fig. 3(a)) while the MWCNTs exhibit straight and smooth layer with better continuation of graphite with the introduction of the Al layer as shown in Fig. 3(b). In addition, the MWCNT grown on the buffer in Fig. 3(b) doesn't display amorphous layer as shown in Fig. 3(a). The amorphous layer and discontinuation point of the CNT in Fig. 3(a) are labeled by black and white arrows, respectively. For the MWCNTs grown on the Si/SiO_2 and Si/SiO_2/Al substrates, our TEM observation indicates that the aluminum buffer layer shows similar effect on improving the morphology and microstructure of the nanotubes. Fig. 5 shows the typical TEM images of the nanotube at the tip and bottom sections, respectively. Fig. 5(a) demonstrates the closed-ended carbon nanotube at the tip while Fig. 5(b) shows that the nanotube grows from the small extrusion of a large catalyst. This finding is similar to the proposed mechanism of the base-growth model [30,31].

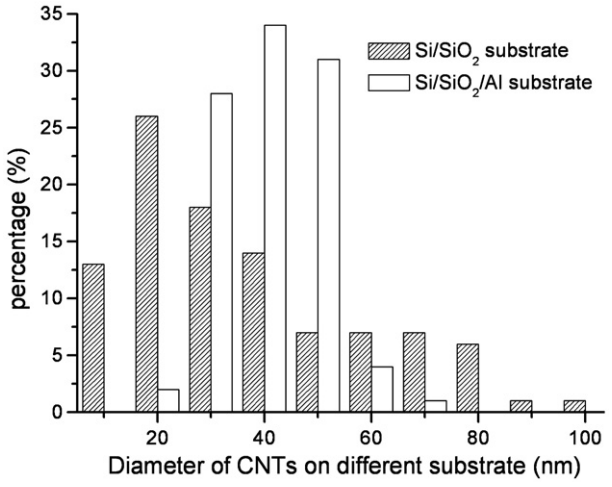

Fig. 4. Diameter distribution of CNTs grown on Si/SiO_2 and Si/SiO_2/Al.

3.2. Chemical state analysis of catalysts by XPS

To achieve increased understanding of the effect of the aluminum buffer layer, it is necessary to investigate chemical state of the catalyst and its interaction with the substrate at the initial growth process. Commonly, XPS is an effective chemical state determination technique. However, rapid growth rate and base-growth mode of the MWCNTs makes it a non-trivial obstacle to trace the initial chemical state of nanotube-catalyst-substrate system. Herein, controlled experiments were designed by solely vaporizing ferrocene on substrate in which initial information of catalyst, substrate as well as the role of carbon containing in the ferrocene can be readily investigated due to the co-existence of hydrocarbon and catalyst during the decomposition of ferrocene. Here we have chosen silicon substrate to study the effect of buffer layer because it is hard to detect the XPS spectrum of MWCNTs on the sample grown on the carbon paper without aluminum buffer. In the experiments, the catalytic ferrocene was vaporized at 850 °C on the Si/SiO_2 and Si/SiO_2/

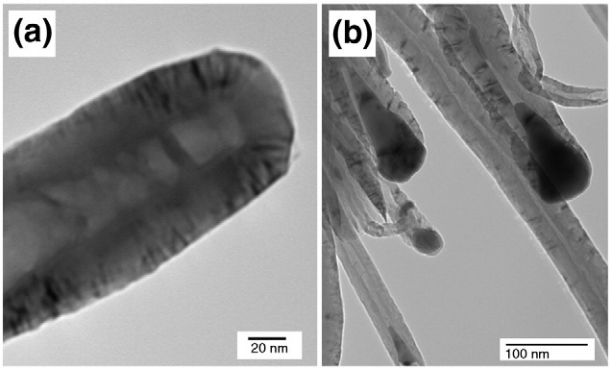

Fig. 5. TEM images of a) MWCNTs having a hollow tip and b) MWCNTs having a big catalyst on the base.

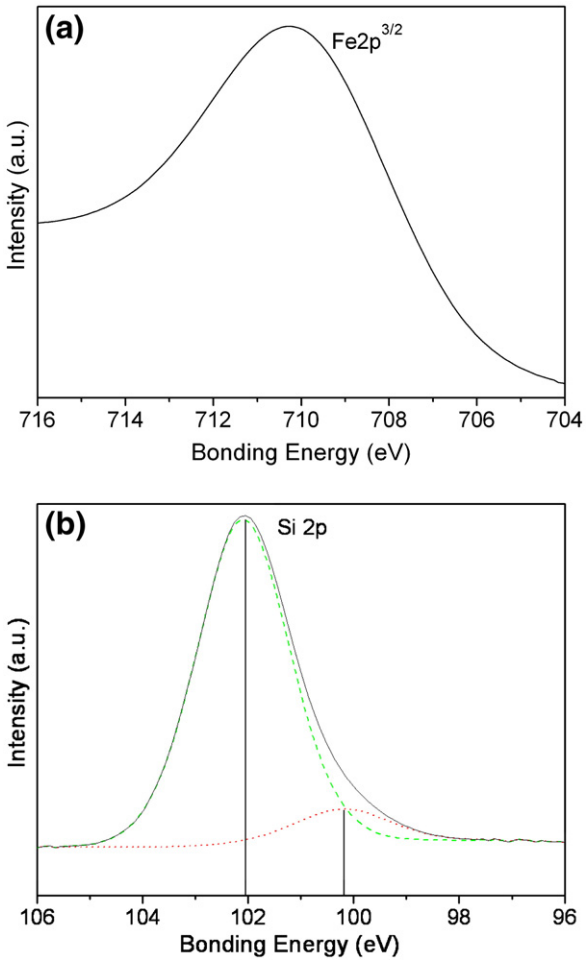

Fig. 6. XPS spectra of (a) Fe $2p^{3/2}$ core level and (b) Si 2p levels obtained from the Si/SiO_2 substrate without the Al buffer.

Al substrates for 2 min and 30 s, respectively, but without introducing extra carbon gas. SEM observations indicated that the growth in 2 min resulted in short (~300 nm) MWCNTs and the growth in 30 s gave shorter nanotubes with the diameter of 30–50 nm. The XPS analysis was conducted on the samples with the nanotubes grown in 30 s. The XPS survey spectra obtained from the samples grown on the two substrates (not shown here) reveal the general chemical state of the involved elements. Both spectra show the presence of graphite-like carbon, displaying binding energy of C1 s at 284.7 eV (with Al layer), 284.5 eV (without Al layer), which corresponds to MWCNTs [32] and hollow carbon fibers [33]. The result indicates that the carbon decomposed from ferrocene induced the nucleation of the tubular product. Further, high resolution XPS spectra analysis was also performed to obtain the exact binding energies of the related elements. Here, we concentrated on investigating the chemical state of Fe, Al and Si elements on the Si/SiO_2 and Si/SiO_2/Al substrate at the initial growth stage to reveal the buffer layer effect, as shown in Figs. 6 and 7.

Without an aluminum buffer layer, the line shape of the Fe2p core level shown in Fig. 6(a) indicates a peak centered at 710.99 eV, which can be attributed to the characteristic peak of magnetite, revealing co-existence of FeO and Fe_2O_3 since magnetite is an inverse spinel crystal containing both ferric (Fe^{3+}) and ferrous (Fe^{2+}) ions in a ratio of 2:1. It is well-known that the ferrocene is decomposed into metal iron, hydrogen and hydrocarbons following the reaction shown as [34]:

$$Fe(C_5H_5)_2 \rightarrow Fe + H_2 + CH_4 + C_5H_6 + \ldots \quad (1)$$

In this process, iron catalyst was oxidized after its release from ferrocene. Fig. 6(b) shows the Si2p spectrum centered at 101.6 eV, which can be fitted to two Gaussian peaks centered at 101.88 eV and 103.88 eV. The two peaks are assigned to (Si,O,C) compound and SiO_2, respectively [35], indicating that there is no formation of silicide which can poison catalyst activity [24]. This suggests that the negative influence of silicide on the nanotube growth can be excluded in our studies.

Interestingly, metal iron was detected while an aluminum buffer layer was employed. The XPS spectrum of the Fe $2p^{3/2}$ core level in Fig. 7(a) exhibits an asymmetric peak centered at 707.00 eV and two Gaussian peaks centered at 710.52 eV and 711.66 eV, respectively. These peaks are assigned to the mixture of metal iron (707.00 eV) [25], magnetite (710.52 eV) [25,36] and iron oxyhydroxide (711.66 eV) [36], respectively. We will

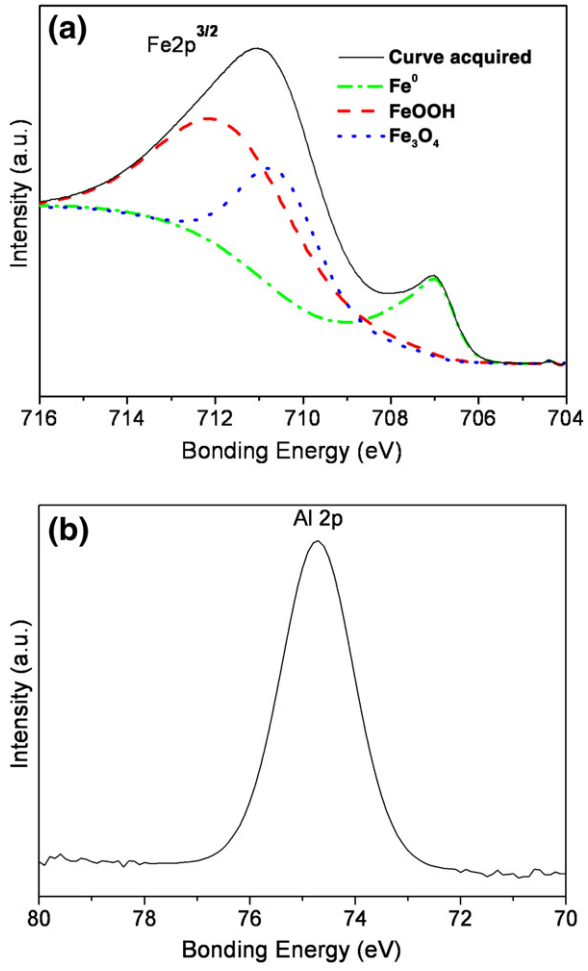

Fig. 7. XPS spectra of (a) Fe $2p^{3/2}$ core levels and (b) Al2p level obtained from the Si/SiO_2 substrate sputtered with the Al buffer.

discuss the generation of metallic iron later. Fig. 7(b) shows the line shape of the Al2p core level, exhibiting a symmetric peak at 74.72 eV, which is identified as Al_2O_3 [37] revealing the existence of an aluminum oxide layer on the surface of the substrate.

3.3. Growth mechanism

Based on the above careful observations and analysis, it has been revealed that introduction of the Al buffer is an important factor in enhancing growth of MWCNTs. Here, we take the growth of the MWCNTs on the silicon oxide/silicon wafer as the example to propose the following model to interpret the buffer layer effect on the MWCNTs growth.

For the $Si/SiO_2/Al$ substrate, the deposition of aluminum by e-beam evaporation usually produces a high roughness due to island growth [38,39], as shown in Fig. 8(a), which is different from the flat substrate. The roughness was enhanced because of alumina formation during the heating process [39] (Fig. 8(b)). It is known that the growth of carbon nanotubes depends considerably on catalyst particle chemical composition and size. While ferrocene was transported into the reaction region, highly active iron and carbon atoms were produced. On the alumina surface, the iron atoms were absorbed into the traps of the alumina layer and were oxidized to form uniform and well dispersed iron oxide particles because of high dispersion effect of alumina (Fig. 8(c)) [40], which is a key factor for growing uniform and aligned MWCNTs. According to the XPS analysis above, it revealed the presence of metallic iron signal on the sample with the Al buffer. It is commonly believed that iron oxide can be reduced to metallic Fe during the CNTs growth and the metallic Fe is the active catalyst form [41]. In this case, the particles would possess a core (iron oxide)/shell (metallic iron) structure. The active metallic iron shell would provide the channel for accumulation and diffusion of the carbon species to feed the carbon nanotube growth, while the oxide core could pin the whole particle to the substrate to favor the base-growth of the carbon nanotubes (Fig. 8d and e) and also improve the bonding between the MWCNTs and the substrate as the previous reports [25,42].

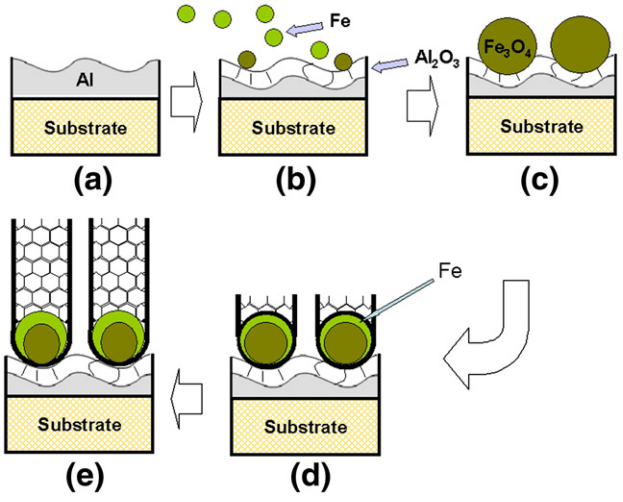

Fig. 8. (a–e) Schematic diagram illustrating the growth mechanism of the CNTs with an aluminum buffer layer.

However, no metallic iron was detected on the sample with only SiO_2 buffer although carbon reduction occurred in the similar way. As is known, iron oxide particles can absorb the carbon species and the reaction between C atoms and O atoms may occur forming CO instead of graphene sheets [43]. Successive reduction of iron oxide particles results in a competitive effect between the formation of graphene sheets and reduction of iron oxide, which demonstrates as a delicate reduction of the iron oxide and low growth rate on the Si/SiO_2 substrate. For the growth on the $Si/SiO_2/Al$ substrate, the decomposition of hydrocarbons could be enhanced by the alumina surface [44], which produced locally high carbon and hydrogen concentration. In addition, strong Al_2O_3/catalyst interaction promotes electron transfer between the substrate and catalyst [45]. Hence, the reduction reaction from iron oxide to iron was significantly promoted. Of course, the XPS result in this paper reveals initial growth stage of the MWCNTs. With the proceeding of continuous reduction reaction of the carbon species, metallic iron may be formed in both cases. Due to capillary effect, the liquid iron catalyst due to oversaturated of carbon [46] is possible to be drawn by the carbon nanotube from the solid parent catalyst particle on the substrate, which coincides with the appearance of catalyst particles in the middle part of the carbon nanotubes in the TEM observation.

It should be noted that some randomly distributed micro-particles were observed on the sample with the Al buffer layer based on the SEM observation in the initial growth stage of the MWCNTs (not shown here). It is known that XPS is a surface sensitive technique with the analysis depth of only a couple of nanometers. Therefore, we employed EDX to detect the composition of the microparticles in-depth. The EDX analysis revealed strong Al and Fe and very weak O signals on the particles, suggesting that the Al layer was only partly oxidized at the surface during the annealing process. In this case (Fig. 8e), the un-oxidized aluminum melted at the target temperature because aluminum has a relatively low melting point of about 660 °C. The melting aluminum might react with the iron oxide particle to generate metallic iron, which may be also a reason why metallic iron was formed for the sample with aluminum buffer. In addition, a Fe–Al alloy was possibly formed. As Nolan et al. reported [47], catalyst activity can be significantly enhanced by alloying a catalyst (i.e., Fe) and a non-catalytic metal (i.e., Al), and both surface and subsurface sites are active in the carbon deposition process. This may be another reason why the presence of Al buffer layer resulted in a higher growth rate and produced neater MWCNTs in our studies. However, we have not got clear evidence to support this assumption yet. Detailed research work has to be deepened in the future to understand exact role of the aluminum buffer.

4. Conclusions

In this paper, we have successfully obtained uniform, clear and aligned MWCNTs by using aluminum as a buffer layer on

both silicon and carbon paper substrates in the floating catalyst CVD method. The growth rate and quality of the MWCNTs have been significantly improved compared to the MWCNTs without using an aluminum buffer layer. Effects of the Al buffer layer on the growth and structure of MWCNTs have been clearly revealed: (i) the Al buffer increases the MWCNTs' growth rate; (ii) the Al buffer layer results in an uniform diameter distribution of the MWCNTs; (iii) the Al buffer layer produces neater MWCNTs with improved crystallinity; and (iv) the Al buffer layer is a crucial factor for the growth of high-density CNTs on carbon paper. Strong catalyst-substrate interaction between the catalyst and Al_2O_3 is thought to be the dominant factor in improving the nanotube growth. In addition, the formation of a Fe–Al alloy is also possible in enhancing reactivity of the catalyst.

Acknowledgements

This research was supported by the Department of National Defense (DND), Natural Sciences and Engineering Research Council of Canada (NSERC), Canada Foundation for Innovation (CFI), Ontario Research Fund (ORF), Canada Research Chair (CRC) Program, Ontario Early Researcher Award (ERA) and the University of Western Ontario. We are in debt to Fred Pearson, Ronad Smith, Mark Biesinger, Ross Davidson and Todd Simpson for their kind help and fruitful discussions.

References

[1] S. Iijima, Nature 354 (1991) 56.
[2] M.M.T. Treacy, T.W. Ebbesen, J.M. Givson, Nature 381 (1996) 678.
[3] M.F. Yu, O. Lourie, M.J. Dyer, K. Moloni, T.F. Kelly, R.S. Ruoff, Science 287 (2000) 637.
[4] J.F. Despres, E. Daguerre, K. Lafdi, Carbon 33 (1995) 87.
[5] S. Iijima, C. Brabec, A. Maiti, J. Bernholc, J. Chem. Phys. 104 (1996) 2089.
[6] S.J. Trans, M. Devoret, H. Dai, A. Thess, R. Smalley, L. Geerligs, C. Dekker, Nature 386 (1997) 474.
[7] M. Bockrath, D. Cobden, P. McEuen, N. Chopra, A. Zettl, A. Thess, R. Smalley, Science 275 (1997) 1922.
[8] D. Cobden, M. Bockrath, N. Chopra, A. Zettle, P. McEuen, A. Rinzler, R. Smalley, Phys. Rev. Lett. 81 (1998) 681.
[9] S. Fan, M. Chapline, N. Franklin, T. Tombler, A. Cassell, H. Dai, Science 283 (1999) 512.
[10] Y.J. Jung, S. Kar, S. Talapatra, C. Soldano, G. Viswanathan, X.S. Li, Z.L. Yao, F.S. Ou, A. Avadhanula, R. Vajtai, S. Curran, O. Nalamasu, P.M. Ajayan, Nano Lett. 6 (2006) 413.
[11] N. de Jonge, Y. Lamy, K. Schoots, T.H. Oosterkamp, Nature 420 (2002) 393.
[12] A.M. Fennimore, T.D. Yuzvinsky, W. Han, M.S. Fuhrer, J. Cumings, A. Zettl, Nature 424 (2003) 408.
[13] W. Huang, S. Taylor, K. Fu, Y. Lin, D. Zhang, T.W. Hanks, A.M. Rao, Y.P. Sun, Nano Lett. 2 (2002) 311.
[14] C. Liu, Y.Y. Fan, M. Liu, H.T. Cong, H.M. Cheng, M.S. Dresselhaus, Science 286 (1999) 1127.
[15] D. Villers, S.H. Sun, A.M. Serventi, J.P. Dodelet, S. De′silets, J. Phys. Chem. B 110 (2006) 25916.
[16] A. Thess, R. Lee, P. Nikolaev, H.J. Dai, P. Petit, J. Robert, C.H. Xu, Y.H. Lee, S.G. Kim, A.G. Rinzler, D.T. Colbert, G.E. Scuseria, D. Tománek, J.E. Fischer, R.E. Smalley, Science 273 (1996) 483.
[17] J. Liu, S.H. Fan, H.J. Dai, MRS Bull. 29 (2004) 244.
[18] Y.Q. Xu, H. Peng, R.H. Hauge, R.E. Smalley, Nano Lett. 5 (2005) 163.
[19] L. Ci, B. Wei, J. Liang, C. Xu, D. Wu, J. Mater. Sci. Lett. 18 (1999) 797.
[20] X. Sun, R. Li, D. Villers, J.P. Dodelet, S. Désilets, Chem. Phys. Lett. 379 (2003) 99.
[21] D. Villers, S.H. Sun, A.M. Serventi, J.P. Dodelet, J. Phys. Chem. B 110 (2006) 25916.
[22] K. Lee, J. Zhang, H. Wang, D.P. Wilkinson, J. Appl. Electrochem. 36 (2006) 507.
[23] Y. Shao, G. Yin, Y. Gao, P. Shi, J. Electrochem. Soc. 153 (2006) A1093.
[24] Y.J. Jung, B.Q. Wei, R. Vajtai, P.M. Ajayan, Y. Homma, K. Prabhakaran, T. Ogino, Nano Lett. 3 (2003) 561.
[25] T.D. Arcos, M.G. Garnier, J.W. Seo, P. Oelhafen, V. Thommen, D. Mathys, J. Phys. Chem. B 108 (2004) 7728.
[26] P.M. Parthangal, R.E. Cavicchi, M.R. Zachariah, Nanotechnology 18 (2007) 185605.
[27] X. Sun, B. Stansfield, J.P. Dodelet, S. Désilets, Chem. Phys. Lett. 363 (2002) 415.
[28] X. Sun, R. Li, B. Stansfield, J.P. Dodelet, S. Désilets, Carbon 45 (2007) 732.
[29] K. Kordesch, G. Simander, Fuel Cells and their Applications, VCH, Germany, 1996, 73.
[30] X. Chen, R. Wang, J. Xu, D. Yu, Micron 35 (2004) 455.
[31] I.K. Song, Y.S. Cho, G.S. Choi, J.B. Park, D.J. Kim, Diamond Relat. Mater. 13 (2004) 1210.
[32] H. Ago, T. Kugler, F. Cacialli, W.R. Salaneck, M.S.P. Shaffer, A.H. Windle, R.H. Friend, J. Phys. Chem. B 103 (1999) 8116.
[33] F. Hoshi, K. Tsugawa, A. Goto, T. Ishikura, S. Yamashita, M. Yumura, T. Hirao, K. Oura, Y. Koga, Diamond Relat. Mater. 10 (2001) 254.
[34] A. Leonhardt, S. Hampel, C. Müller, I. Mönch, R. Koseva, M. Ritschel, D. Elefant, K. Biedermann, B. Büchner, Chem. Vap. Depos. 12 (2006) 380.
[35] M. Pinault, M.M. L'Hermite, C. Reynaud, V. Pichot, P. Launois, D. Ballutaud, Carbon 43 (2005) 2968.
[36] Y.S. Min, E.J. Bae, J.B. Park, W.J. Park, Nanotechnology 17 (2006) 116.
[37] Z.K. Tsameret, A. Raveh, J. Vac. Sci. Technol. A 13 (1995) 1121.
[38] I.T. Han, B.K. Kim, H.J. Kim, M. Yang, Y.W. Jin, S. Jung, N. Lee, S.K. Kim, J.M. Kim, Chem. Phys. Lett. 400 (2004) 139.
[39] K.Y. Lee, S.I. Honda, M. Katayama, T. Miyake, K. Himuro, K. Oura, J.G. Lee, H. Mori, T. Hirao, J. Vac. Sci Technol. B 23 (2005) 1450.
[40] J.H. Anastasios, H.S. Alexander, R. Laure, Carbon 44 (2006) 348.
[41] Y. Homma, Y. Kobayashi, T. Ogino, D. Takagi, R. Ito, Y.T. Jung, P.M. Ajayan, Jpn. J. Appl. Phys. 107 (2003) 12161.
[42] N. Ishigami, H. Ago, Y. Motoyama, M. Takasaki, M. Shinagawa, K. Takahashi, Chem. Commun. (2007) 1626.
[43] A. Moisala, A.G. Nasibulin, E.I. Kauppinen, J. Phys. Condens. Matter 15 (2003) S3011.
[44] R. Seidel, G.S. Duesberg, E. Unger, A.P. Graham, M. Liebau, F. Kreupl, J. Phys. Chem. B 108 (2004) 1888.
[45] W.R. Vander, T.M. Ticich, V.E. Curtis, Carbon 39 (2001) 2277.
[46] O.P. Krivoruchko, V.I. Zaikovskii, Kinet. Catal. 39 (1998) 561.
[47] P.E. Nolan, D.C. Lynch, A.H. Cutler, J. Phys. Chem. B 102 (1998) 4165.